Vol.66: e23220408, 2023
https://doi.org/10.1590/1678-4324-2023220408
ISSN 1678-4324 Online Edition

BABT
BRAZILIAN ARCHIVES OF BIOLOGY AND TECHNOLOGY

Article - Engineering, Technology and Techniques

Design and Analysis of Different Locking Mechanisms for Stand-alone Posterior Lumbar Cage Implant

Sathya Bharathy Sathyanathan[1]
https://orcid.org/0000-0003-4521-9869

Sudhir Ganesan[2]
https://orcid.org/0000-0003-1743-2865

Kavitha Anandan[3]
https://orcid.org/0000-0002-3890-6399

[1]Loyola-ICAM College of Engineering and Technology, Department of Electrical and Electronics Engineering, Chennai, Tamil Nadu, India; [2]Sri Ramachandra Medical Centre, Department of Orthopaedics, Chennai Tamil Nadu, India; [3]Sri Sivasubramaniya Nadar College of Engineering, Department of Biomedical Engineering, Chennai, Tamil Nadu, India.

Editor-in-Chief: Alexandre Rasi Aoki
Associate Editor: Alexandre Rasi Aoki

Received: 11-June-2022; Accepted: 14-Feb-2023.

*Correspondence: kavithaa@ssn.edu.in; Tel.: +91-9677057669 (K.A.).

HIGHLIGHTS

- Design of Artificial Inter Vertebral Discs with self-locking mechanism.
- Elimination of rods and plates that require additional penetration and space in vertebrae.
- Stress-Strain Analysis of the proposed designs.
- Results show that proposed design would provide stability for functional spinal units.

Abstract: Spinal implants are commonly used in the treatment of spinal disorders and injuries. Spine surgery for interbody fusion using intervertebral cages has become a prescribed method to treat degenerative disc disease and spondylolisthesis. Interbody fusion cages restore disc height by replacing the degenerated disc. Cage design, the material and the surgical approach play significant roles in a successful clinical outcome. A cage implant provides stability for functional spinal units; however, this is accomplished with rods and plates that require additional penetration and space in vertebrae. Hence, stand-alone cage devices are being used, but the designs and their effectiveness are still investigational. This work aims at designing intervertebral cage models with a self-locking mechanism. Four prospective designs for the locking mechanism are proposed. The design is modeled using SOLIDWORKS®. The mechanical analysis was performed on the modeled implants using ANSYS. The material of the implant is titanium, based on its proven biomechanical properties. The dimensions of the cage implant were chosen to best suit the lumbar L4/5 Intervertebral Disc (IVD). Analysis of results indicates that the proposed designs with the locking mechanism withstand load and provide stability to functional spinal units. The modeled cage implants with the proposed locking mechanism show prospective results from mechanical analysis and proceed further for biomechanical testing.

Keywords: Intervertebral Disc; Spinal Implant; Biocompatible; Finite Element Analysis.

INTRODUCTION

About eighty percent of the adult population is affected by low back pain [1-4]. This musculoskeletal pathology may be due to changes in the vertebrae or the intervertebral disc (IVD). The problems associated with IVD are disc degeneration, bulging, herniation and thinning that can result in back pain, sciatica and neural compression [3]. In the subjects where medication fails and the IVD needs to be replaced, surgical treatment is used, in which the IVD will be removed and replaced with an artificial disc (AD) or a cage implant fused with bone grafts [4]. Surgical techniques for lumbar and cervical discs involve replacing IVD with a cage implant with a bone graft to uphold bone growth and fusion with vertebrae [5]. The cage implant should also be accompanied by rods and pedicle screws to lock and prevent the movement of the cage between the vertebrae. Thus, additional procedures would be required on the spinal bone while placing the cage, to accommodate the rods and screws. The biocompatibility and biomechanical characteristics of this additional hardware need to be analyzed from time to time postoperatively. To reduce the use of additional hardware inside the body, the need to design stand-alone intervertebral cages with self-locking mechanisms has recently gained importance [6-8]. This study aims to design anatomical stand-alone lumbar cage implants with a self-locking mechanism and analyze their mechanical characteristics to support interbody fusion [4-6]. The L4 and L5 vertebrae experience a higher load during spinal activities leading to a higher possibility for L4/5 IVD degeneration [3-4]. Hence, the dimensions of the proposed implant were chosen to best suit the lumbar L4/5 IVD.

MATERIAL AND METHODS

Design of Lumbar Intervertebral Implant

Novel designs of cage implants were developed by analyzing the anatomy of the lumbar spine and disc. The implant was designed based on the shape and dimension of the lumbar spine and the space available between the vertebrae after removing the disc [9]. The design is intended for the posterior approach and has two parts, the cage part that forms the base and the self-locking mechanism [4][6], which is the primary objective of the new design. The proposed designs of the implant were modeled using SOLIDWORKS®. Material properties of the various biomaterials were analyzed from the literature, and titanium (Ti) was found to support the biomechanical factors required and hence selected as the material for the proposed design of the implant [10-12]. Though *Ti* has a few disadvantages, its bioactivity can be improved by modifying its surface topography and subjecting it to physical and chemical treatment, creating a porous material with high interconnectivity [11][13]. Load analysis [14-15] was performed on the modeled implant designs using ANSYS to evaluate its mechanical behavior.

The design of the implant consists of two major parts. The first part is the cage, designed to replace the IVD. The second part is the self-locking mechanism (SLM) to create fixation of the cage with the Lumbar vertebra to arrest the movement of the cage.

Design of cage

The proposed design of the implant was conceived for a posterior approach of interbody fusion. The geometry of the cage includes an aerodynamic profiled front part for easy insertion of the implant into the intervertebral space. The implant dimensions are designed by considering the average dimension of the IVD that the implant would replace between two adjacent vertebrates of the adult lumbar section [9]. The dimensions of the L4/5 disc [9] and that of the cage implant are given in Table 1. A cavity is provided in the cage design to accommodate the bone graft to augment interbody fusion [5]. The upper and lower surfaces of the cage are provided with saw-tooth cuttings to facilitate a firm clutch into the adjoining vertebrae.

The basic requirement of a stand-alone implant for lumbar IVD replacement is the rigid fixation of the implant with the associated spinal bones. Hence, four different locking mechanisms, Model-1(M1), Model-2(M2), Model-3(M3) and Model-4(M4), are proposed in this work, to assess the efficient fixation of the implant. Based on the locking mechanism, two different cage models are designed. The modeled cage part shown in Figure 1 is common for both M1 and M2.

Table 1. Dimensions of the L4/5 disc and the implant model

	L4/5 disc (mm)	Cage dimension (mm)			
		M1	M2	M3	M4
Length	26.4 – 46.2	26	26	24	24
Width	46.17 ± 4.7	18	18	12	12
Height	11.3±2.1	12	12	12	12

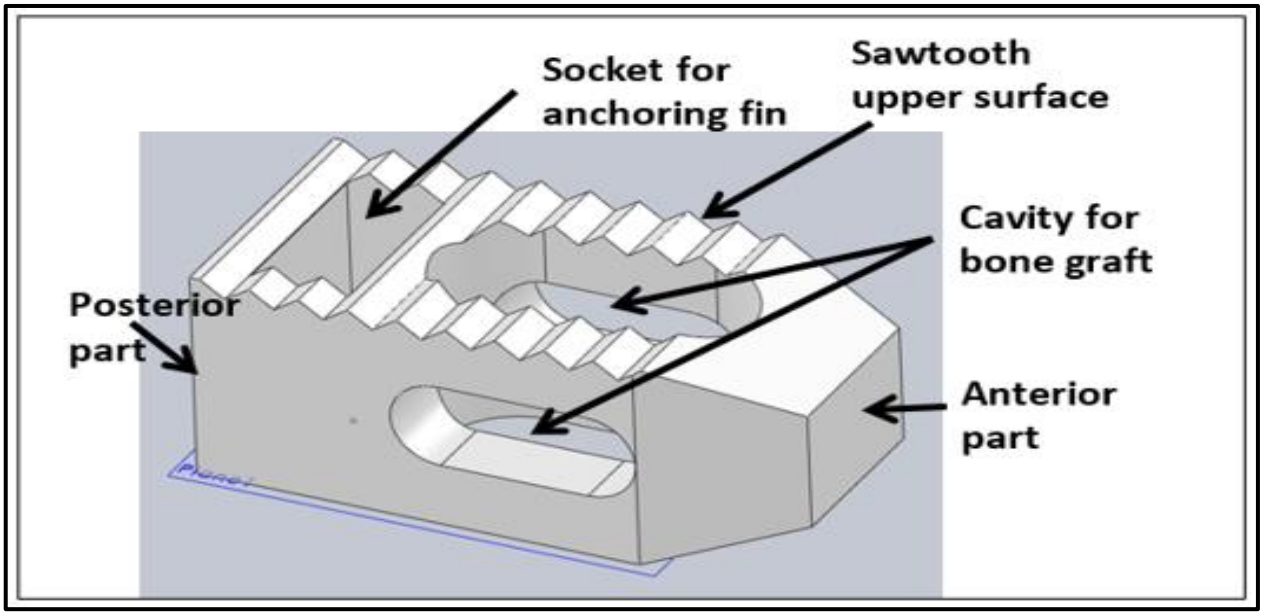

Figure 1. Three-dimensional model of cage part of the implant

The biomaterial titanium alloy was chosen for the cage body based on its proven biocompatibility, physical and mechanical properties [10-12]. Thirty percent of the implant volume consists of a cavity to facilitate a cancellous bone graft insertion and growth, thereby accelerating interbody fusion. In the proposed designs the cavity holds approximately an equal amount of bone graft. In addition, uniform height or thickness was maintained from the anterior to the posterior of the implant to accommodate lordosis in the lumbar region.

Design of Self-Locking Mechanism (SLM)

The objective of the new design is to provide a self-locking mechanism with the cage. Four methods/models of the locking mechanism are proposed in this work.

Design of SLM –M1: Gear-Screw Model

The three-dimensional (3D) model of the Gear-Screw design is shown in Figure 2 and Figure 3. The socket, provided at the posterior part of the cage, holds a mini gear between two spearhead flat screws FS1 and FS2. The flat screws are designed with a spearhead to facilitate penetration into the spinal bones. The other end was blunted to prevent further penetration. The spearhead of FS1 is pointed upward and that of FS2 downward. The side faces of FS1 and FS2 are flat, and the face of each of the screws has teeth to make contact with the gear teeth. The operation between the gear and the flat locking screws is based on the rack and pinion principle. On instrumented clockwise rotation of the mini gear about its axis, the spearheaded FS1 and FS2 simultaneously penetrate the upper and lower spinal bones and achieve locking of the AD with the vertebrae. The locking screws are expected to provide sufficient stability to the cage implant. The cage and the locking screws accommodate the space between the vertebrae, preventing irritation or impingement upon neighboring visceral structures and nerves.

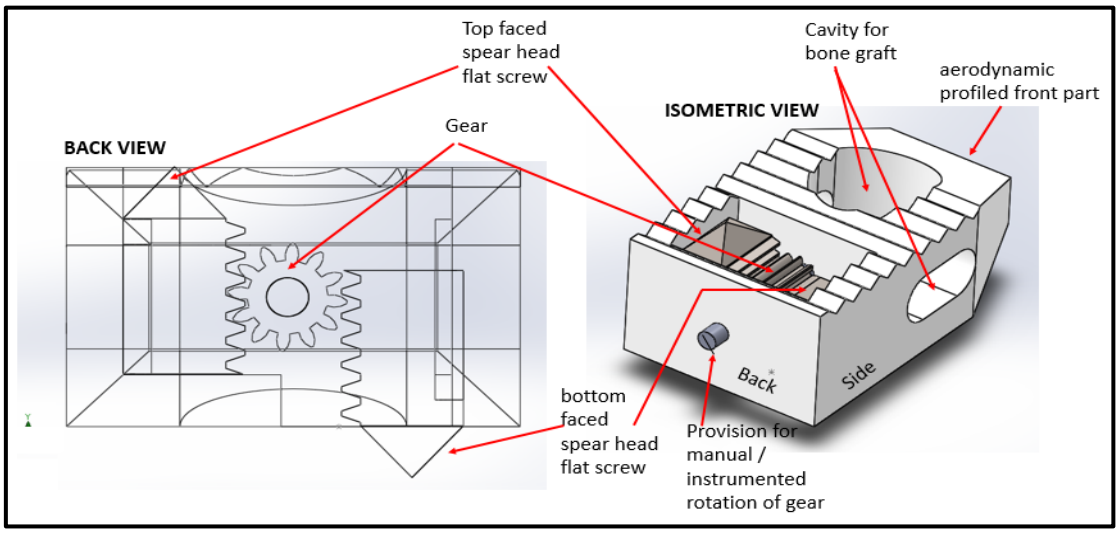

Figure 2. Design of SLM- Model-1

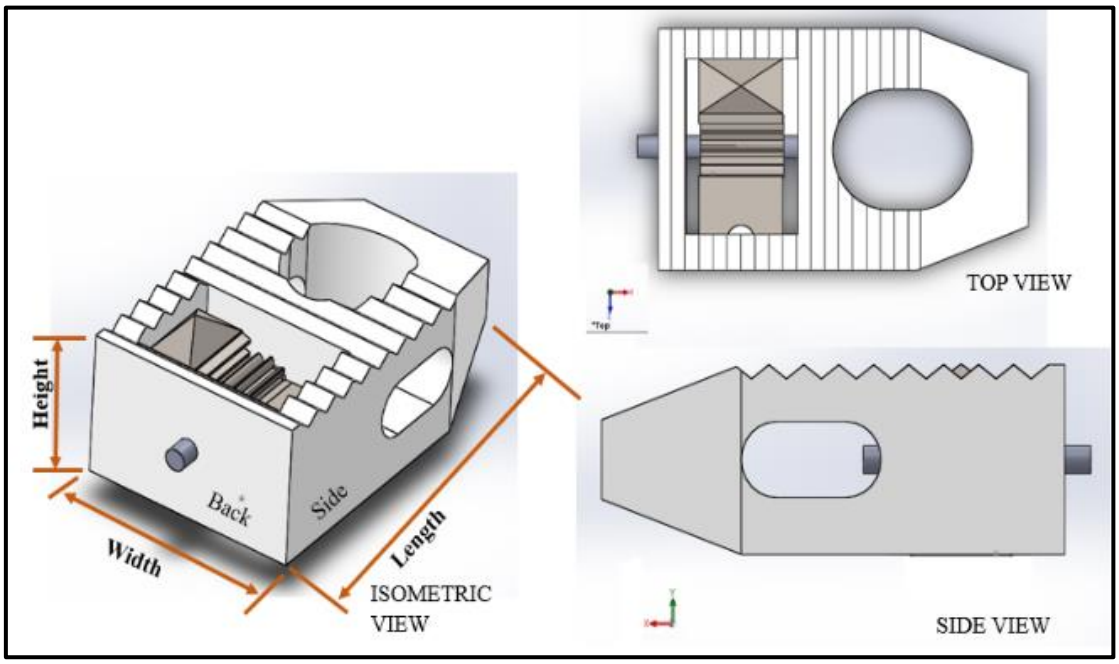

Figure 3. Three-dimensional model of cage implant for model-1: Isometric view (left), Top view (top right) and Side view (bottom right)

Design of SLM –M2: Spring-Fin Model

An alternate locking mechanism is proposed in model-2, the Spring-Fin model, shown in Figure 4. There is no change in the dimensions of the cage part. Two anchoring fins AF1 and AF2, with coil springs, are provided inside the socket to lock AD with the spinal bone. The spring of the AF1 is fixed to the socket's bottom surface, and the anchoring fin at its top faces upward to make a fixation with the upper vertebra. The spring of the anchoring fin-2 is fixed to the socket's top surface and its anchoring fin faces downward to make fixation with the lower vertebra. Thus, the anchoring fins remain firmly locked inside the socket during implant placement between the two lumbar spines. The spring has a plate bottom and a projecting button to lock the spring in a compressed position. On applying a small force on the button, the spring is released from compression, and the anchoring fin penetrates the lumbar bones and arrests the movement of the cage implant. The Back view, Side view, Top view and Isometric view of the Spring-fin model with its locking mechanism are shown in Figure 4 – (A), (B), (C) and (D) respectively.

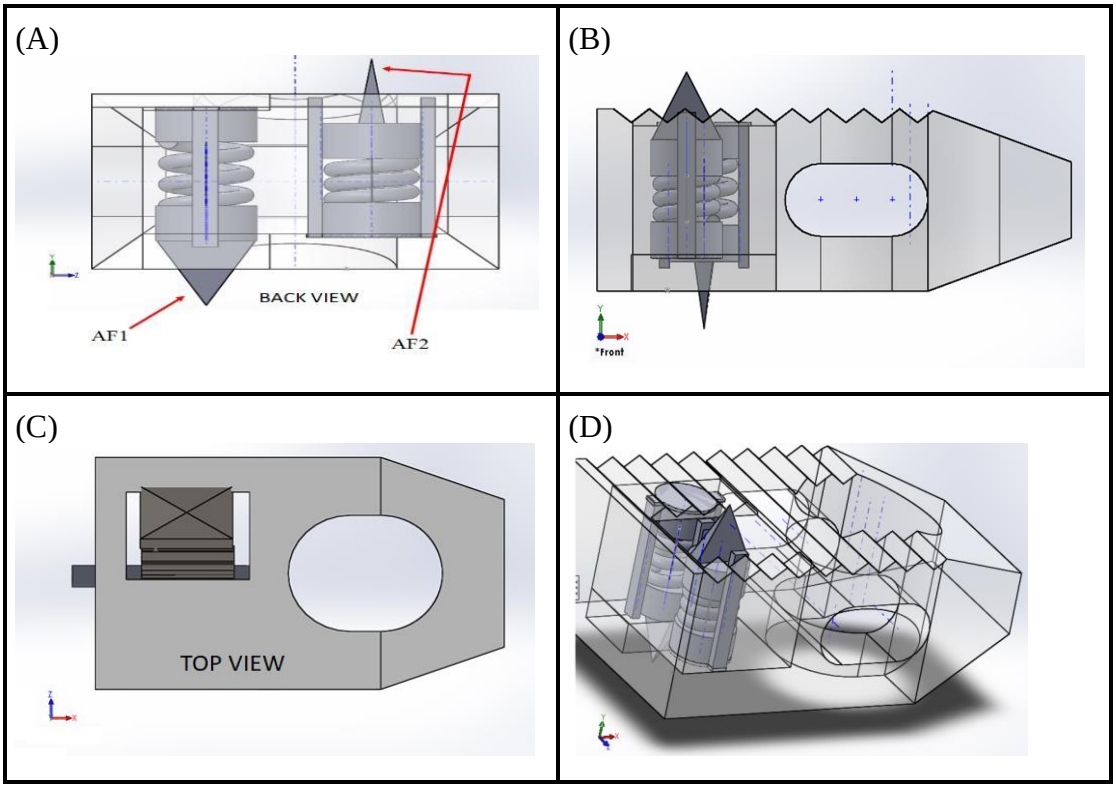

Figure 4. Three-dimensional model of cage implant for SLM-M2: (A)Back view, (B)Side view, (C)Top view, (D)Isometric view.

Design of SLM – M3: Slide-Screw Model

The slide screw model shown in Figure 5(A) consists of the main screw with smooth tapering and two sub-screws to penetrate the upper and lower vertebral bone. One end of the sub-screws has a sharp point to penetrate the spinal bone for locking, and the other end has an inclined cut. Figure 5(B) shows the main screw from the back view of the model. The inclination angle of the main screw and the sub-screws are so designed that the top and bottom sub-screws move upward and downward respectively, when the main screw is moved forward as shown in Figure 5(C). The Figure 5(D) displays the slide screw model with its sub-screws screwed to their locking positions.

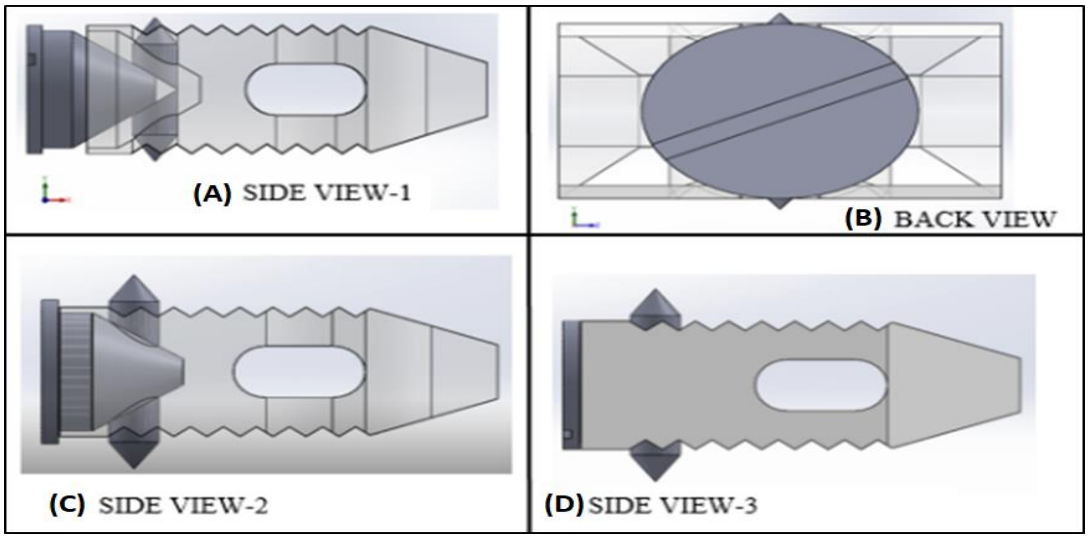

Figure 5. Three-dimensional model of cage implant for SLM-M3: (A) Side view-1 (B) Back view, (C) Side view-2, (D) Side view-3.

Design of SLM – M4: Inc-Screw Model

The Inc-Screw model presented in Figure 6, was designed with a solid cage part and two inclined screw holes are provided from the back face, one proceeding upward and the other downward as shown in Figure 6(A). The top view of the model is given in Figure 6(B). Two screws were designed to screw through the holes provided at the back face, as displayed in Figure 6(C)&(D), to lock the cage implant with the vertebra.

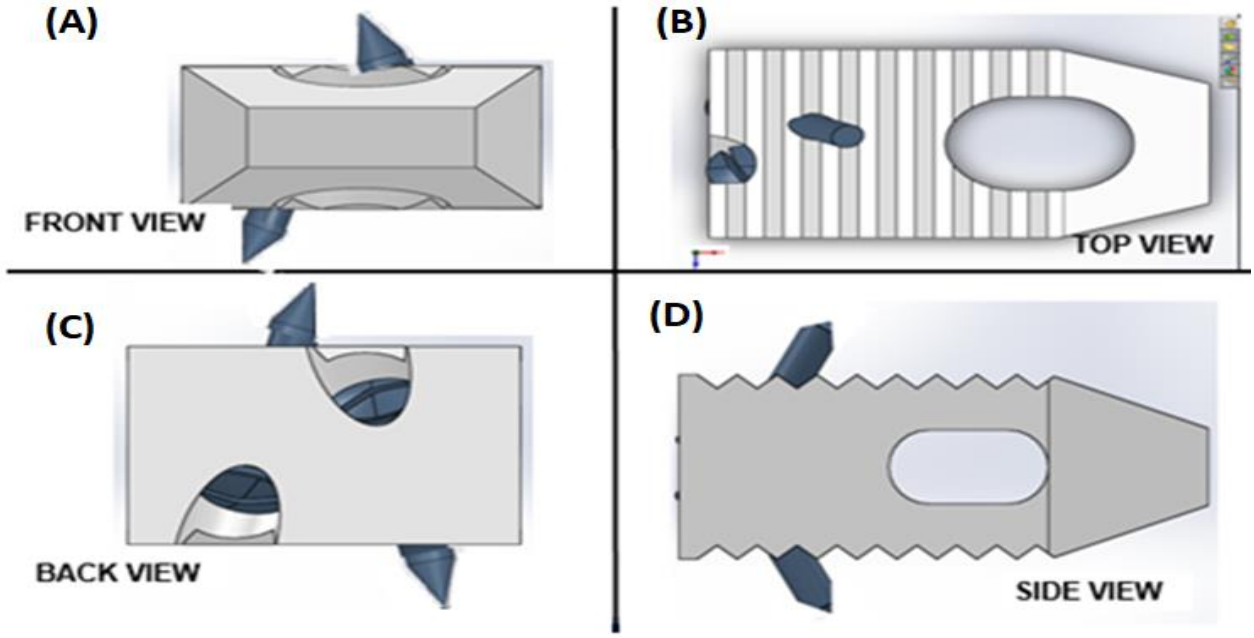

Figure 6. Three-dimensional model of cage implant for SLM-model-4: (A) Front view, (B) Top view, (C) Back view, (D) Side view

Mechanical Analysis

Mechanical Analysis is a series of tests performed to test how the materials and structures react under force or pressure. The primary test was performed to check the stress-strain characteristics [15-16] for the given load on these novel designs. The 3D model of the proposed designs was subjected to compressive load[15-16] to verify its stability. The possibilities for deformations were also studied.

Load versus stress distribution analyses were performed using ANSYS. The body of the cage was applied with the material properties of Titanium. Literature shows that the mechanical analysis on spinal implants could be tested with a compressive load varying from 400N to 1000N [17-19]. Therefore, compressive load values from 600N [20-21] to a maximum of 1.5KN were given to test for any displacement or deformation of the design. The force was applied perpendicular to the direction of the implant. The boundary conditions were applied to restrain the bottom part of the implant.

RESULTS AND DISCUSSION

The stress distribution, principal strain and deformation parameters that were observed using ANSYS, for the maximum load of 1500N on the four models are shown in Figure 7. Three iterations had been performed and the variation in results was found to be $\pm$1E-05 on an average and hence negligible. The M1 and M2 models have shown a similar stress distribution pattern and that of model M3 is similar to M4. The minimum and the maximum values of the stress, strain and deformation observed from the analysis are given in Tables 2, 3 and 4, respectively. The deformation results show the material deformation that occurs on the implant.

The characteristic graphs shown in Figures 8, 9 & 10 depict the changes in stress, strain and deformation values respectively, on all four models during application of the load.

The simulation results of the stress analysis, presented in Figure 7, show that the major part of the implant body of models M1 and M2 experience very minimum stress, illustrated in dark-blue shade and that of models M3 and M4 experience a higher stress illustrated in light-blue shade, but much below the maximum stress. The maximum stress was observed in very minimum certain locations in all four models.

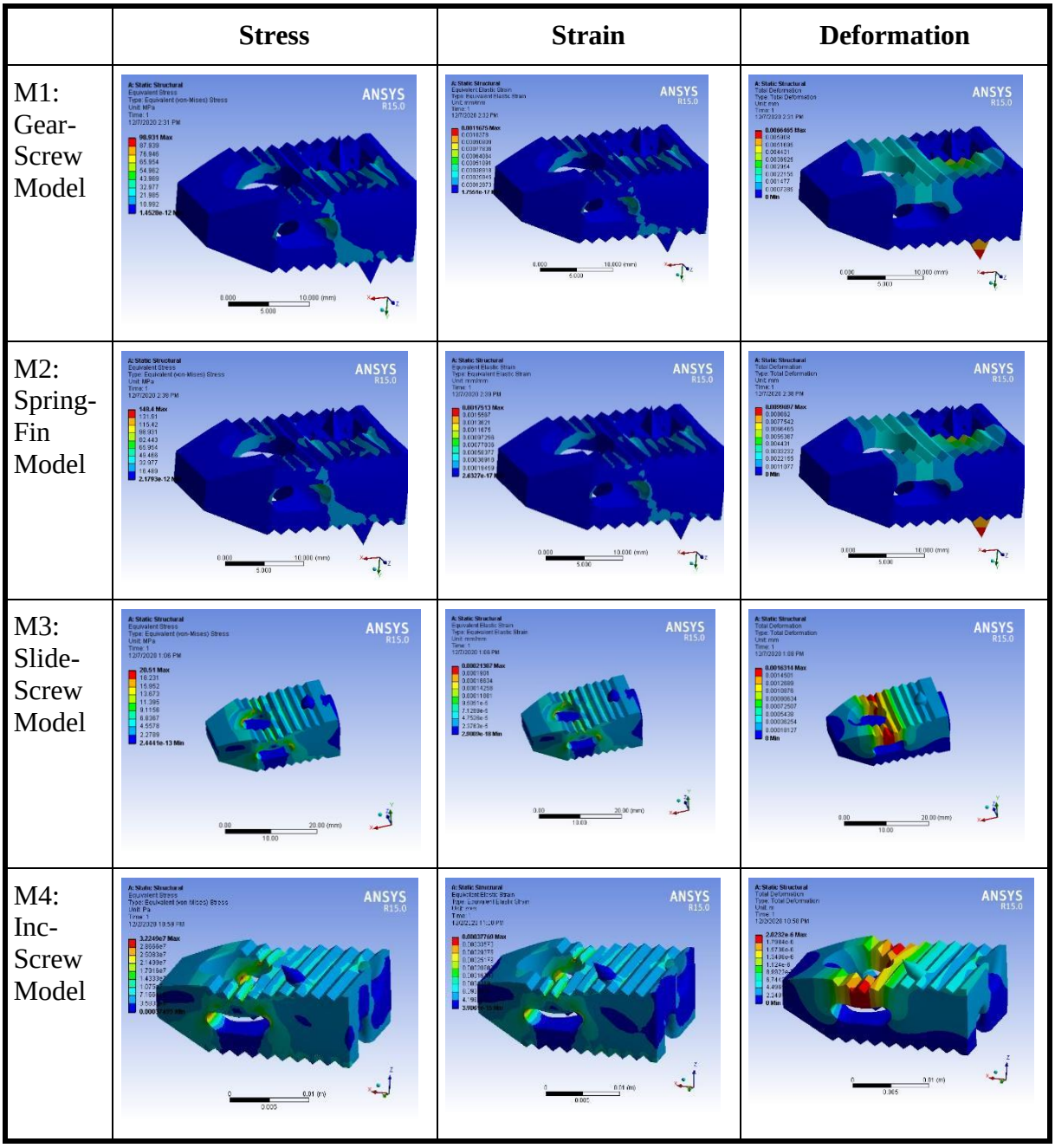

Figure 7. Results of Von mises stress, principal strain and deformation analysis in ANSYS under Static load on Model-1,2,3 & 4.

The minimum and maximum stress experienced by the four models, for the various loads of 600N, 800N, 1000N, 1200N, 1400N and 1500N are presented in Table 2. For the minimum applied load (600 N), maximum stress of 56.378, 59.359, 12.306, 12.9 (MPa) and for the maximum load (1500 N), 145.274, 148.4, 30.765, 32.25 (MPa) were found on M1, M2, M3 and M4, respectively. As per predicted stress values for the simulation benchmark, the maximum von Mises stress allowable in the implant is 25 MPa for 610 N [14]. Comparing the obtained stress values with the benchmark, it was found that the models M1 and M2 are experiencing stress above the limit at certain minimum locations. The maximum stress value (red shades) in M1 and M2 was observed in the inner aspect of the cavity, provided for bone graft. The model M1 experiences maximum stress also in the socket part (posterior part) of the cage where the gear was housed and M2 was found to have in the spring and its fin that was provided to penetrate the lower bone. The posterior part of M1 and M2 exhibits only minimum stress (blue shades), which is lower than the benchmark. Therefore, the models M1 and M2 displayed a value beyond the benchmark only at 4% of the total volume. The models M3 and M4 experience stress well below the allowable limit in its entire volume. Analyzing the acquired stress values in the developed implant designs, using the graphs shown in Figures 8 and 9, it is evident that the models, M3 and M4 are undergoing very low stress compared to M1 and M2.

Table 2. Stress distribution on the implant body for various loads.

Stress Distribution (MPa)												
Load	600N		800 N		1000N		1200 N		1400 N		1500 N	
Model	Min	Max	Min	Max	Min	Max	Min	Max	Min	Max	Min	Max
M1	8.59E-13	56.378	1.01E-12	76.236	1.29E-12	95.758	1.54 E-12	114.72	1.83E-12	134.5	1.99E-12	145.274
M2	8.72E-13	59.359	1.16E-12	79.145	1.45E-12	98.931	1.74 E-12	118.72	2.03E-12	138.5	2.18E-12	148.4
M3	1.47E-13	12.306	1.96E-13	16.408	2.44E-13	20.51	2.93 E-13	24.612	3.42E-13	28.71	3.67E-13	30.765
M4	1.50E-10	12.9	2.50E-10	17.199	3.00E-10	21.499	3.50 E-10	25.799	3.75E-10	30.099	12.9	32.25

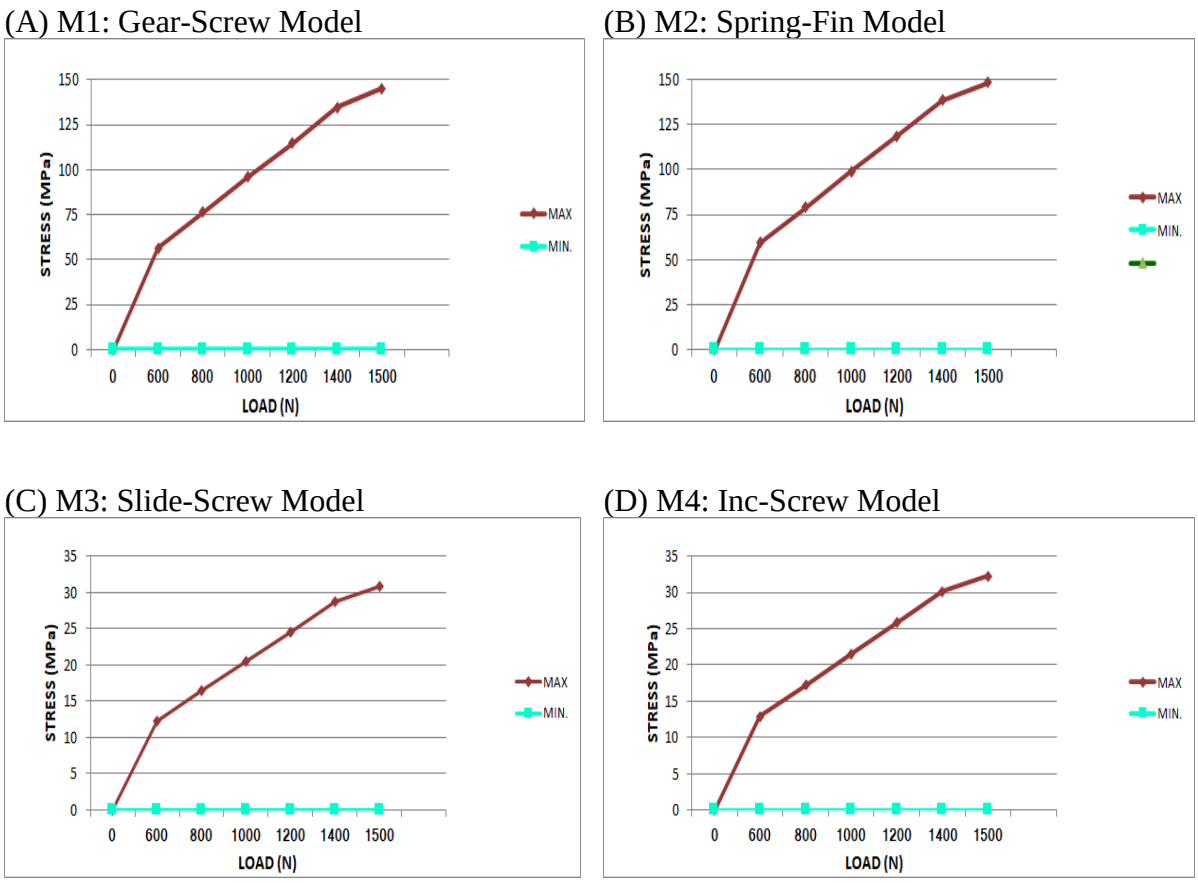

Figure 8. Variations in stress distribution in the models (A) M1 (B) M2 (C) M3 (D) M4.

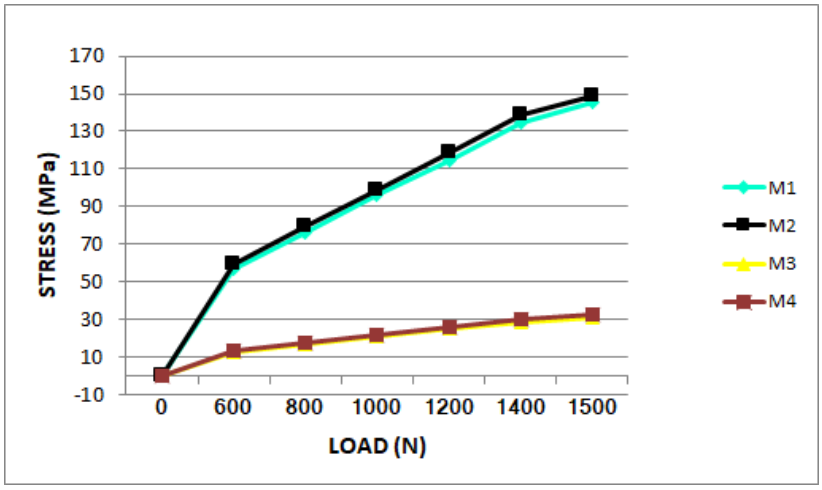

Figure 9. Comparison of stress curves in all four models.

The simulation results of strain analysis shown in Figure 7 depict that all the models were subjected to a minimum strain (blue shades) on loading. The minimum and maximum strain endured by the four models, for the various loads ranging from 600N to 1500N are presented in Table 3. The strain(mm/mm) values show minimum values of 1.01E-17, 1.05E-17, 1.74E-18 and 1.56E-14 for a load of 600 N ranging to a maximum strain of 1.69E-03, 1.75E-03, 3.21E-04, 3.78E-04 for a load of 1500 N in the models M1, M2, M3 and M4 respectively. The graph given in Figure 10 shows that the maximum strain that occurred was 1.75E-03 in M2 and the next in order was M1 with 1.69E-03 for the load 1500 N. The observed maximum strain values are below the permissible limits. The comparison of strain curves in the four models given in Figure 11 shows that the models M3 and M4 undergo very minimal strain.

Table 3. Principal strain variations for various loads

	Strain (MM/MM)											
Load	600N		800 N		1000N		1200 N		1400 N		1500 N	
Model	Min	Max	Min	Max	Min	Max	Min	Max	Min	Max	Min	Max
M1	1.01E-17	6.05E-04	1.36E-17	8.43E-04	1.65E-17	1.06E-03	2.06E-17	1.32E-03	2.38E-17	1.58E-03	2.59E-17	1.69E-03
M2	1.05E-17	7.01E-04	1.40E-17	9.34E-04	1.76E-17	1.17E-03	2.11E-17	1.40E-03	2.46E-17	1.63E-03	2.63E-17	1.75E-03
M3	1.74E-18	1.28E-04	2.32E-18	1.71E-04	2.90E-18	2.14E-04	3.48E-18	2.57E-04	4.06E-18	2.99E-04	4.35E-18	3.21E-04
M4	1.56E-14	1.51E-04	2.08E-14	2.01E-04	2.60E-14	2.52E-04	3.12E-14	3.02E-04	3.65E-14	3.53E-04	3.91E-14	3.78E-04

(A) M1: Gear-Screw Model

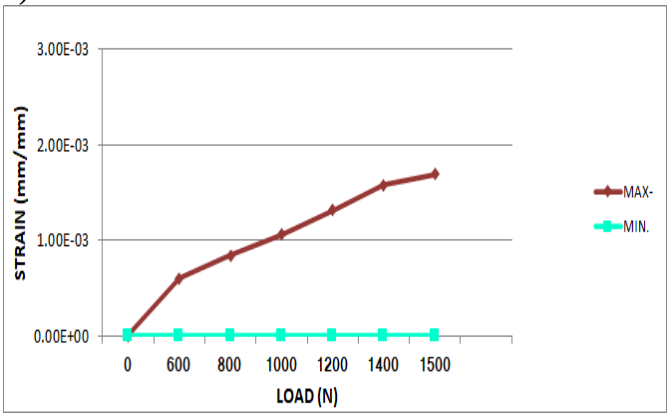

(B) M2: Spring-Fin Model

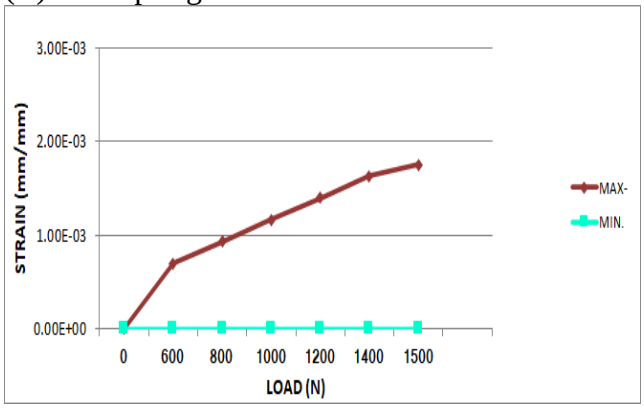

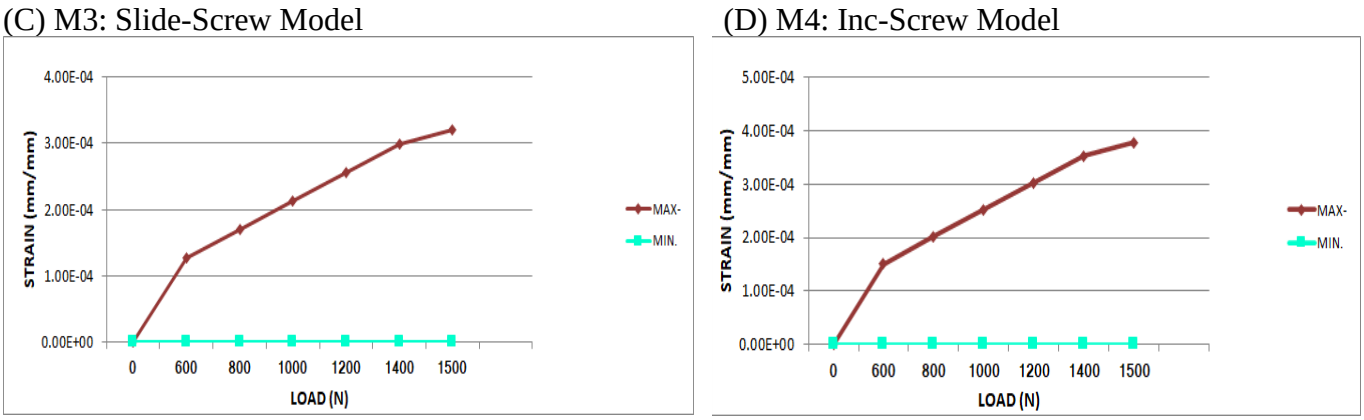

Figure 10. Principal strain in the models (A) M1 (B) M2 (C) M4 (D) M4

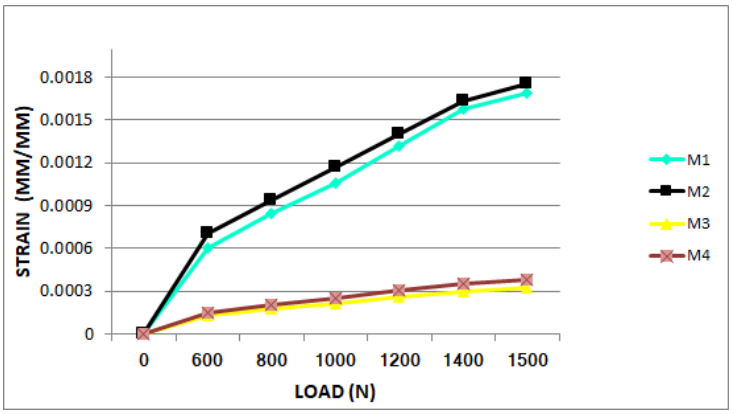

Figure 11. Comparison of strain curves in all four models.

The values of deformation(mm) experienced by the four models are presented in Table 4. For the loads 600N to 1500N, a minimum of zero deformation and a maximum of 9.36E03, 9.97E-03, 2.04E-03 and 2.02E-03 were observed in the models M1, M2, M3 and M4 respectively. The minimum and maximum deformation characteristic curves for the four models are presented in Figure 12. Due to the maximum stress distributed at the gear part of M1 and lower spring-fin part of M2, the areas at the said parts experience a deformation. Hence, it was found that in the Gear-screw (M1) model, the part where the gear and its screw make contact needs refinement. Also, it is realized that the gear ratio should be reworked. And in the spring-fin (M2) model, the fixation of the spring with the implant should be constructed more rigidly.

In the models M3 and M4, minimum deformation is observed on 96% of its total volume but the remaining 4% exhibits maximum deformation (red shades). The simulation results for deformation in the models M3 and M4 given in Figure 7 show the maximum deformation on the section of the walls around the cavity provided for bone graft. Hence, the said section needs to be strengthened, though improved strength would be achieved from the inclusion of bone graft. The comparison of maximum deformation in all four models given in Figure 13 shows that the maximum deformation is observed on models M3 and M4 at its screw fixation points are comparatively lower than that on M1 and M2.

Table 4. Variation in deformation observed for the applied loads on the four models

Deformation (MM)												
Load	600N		800 N		1000N		1200 N		1400 N		1500 N	
Model	Min	Max	Min	Max	Min	Max	Min	Max	Min	Max	Min	Max
M1	0	3.87E-03	0	5.02E-03	0	6.39E-03	0	7.67E-03	0	9.18E-03	0	9..36E03
M2	0	3.99E-03	0	5.32E-03	0	6.65E-03	0	7.98E-03	0	9.31E-03	0	9.97E-03
M3	0	8.16E-04	0	1.09E-03	0	1.37E-03	0	1.63E-03	0	1.90E-03	0	2.04E-03
M4	0	8.09E-04	0	1.08E-03	0	1.35E-03	0	1.62E-03	0	1.89E-03	0	2.02E-03

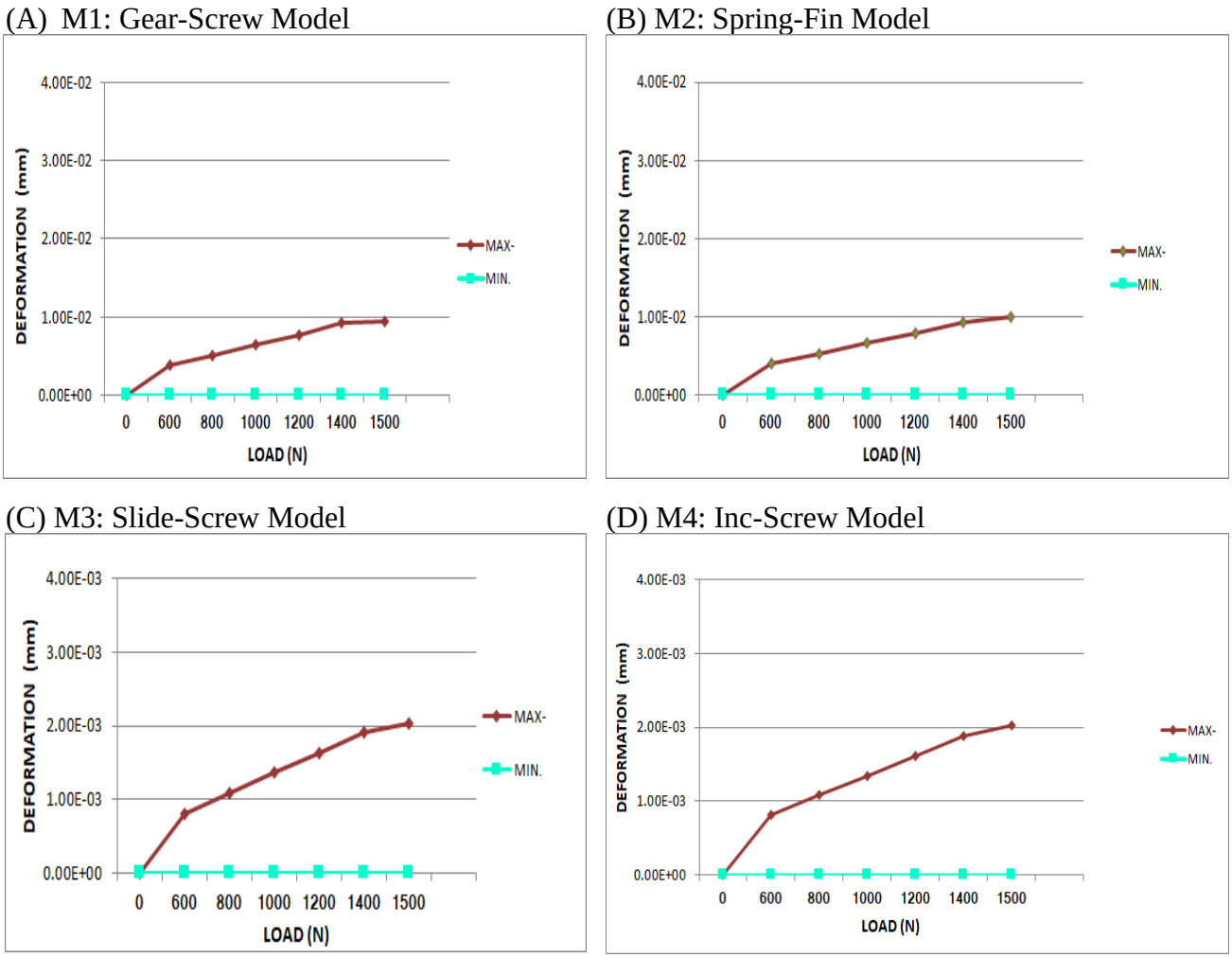

Figure 12. Minimum and Maximum deformation curves for (A) M1 (B) M2 (C) M3 (D) M4

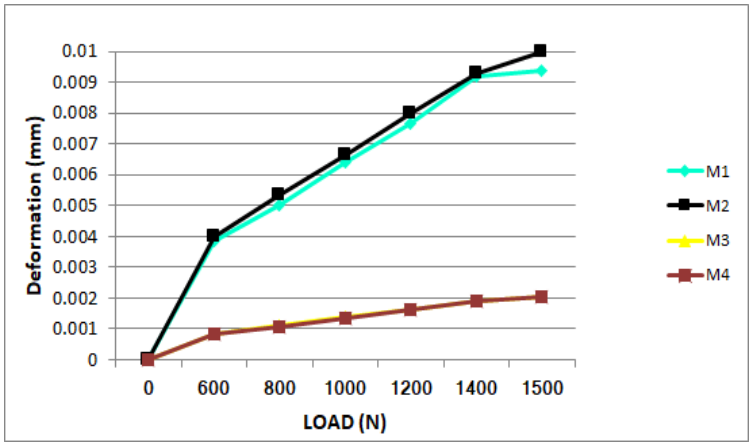

Figure 13. Comparison of characteristic deformation in all four models.

The stress-strain relationship given in Figure 14 shows that the stress-strain curve is within the elastic limit in all four models for the applied range of loads. Hence, all the models exhibit high yield strength, resilience and toughness. M3 and M4 possess higher mechanical properties than M1 and M2. This is because the screws designed for fixation in M3 and M4 are cylindrical screws of higher thickness and provide more stability. Thus it is observed that the mechanical strength of the models M1 and M2 could be improved with a few design modifications.

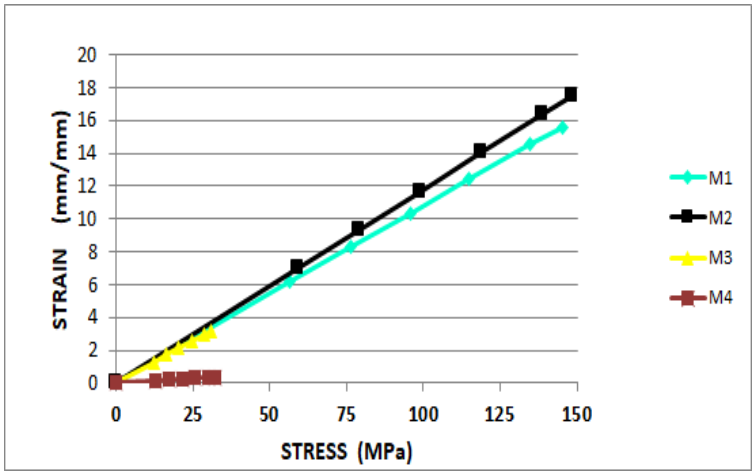

Figure 14. Stress-Strain relationship in all four models.

CONCLUSION

The developed models exhibited satisfactory mechanical behavior and hence could be subjected to biomechanical testing with modeled vertebrae in the subsequent work. Based on the study outcome, further analysis and modifications for improvements could be planned.

Based on the mechanical analysis results, it was found that the model, Gear-screw (M1), requires refinement in design in the part where the gear and its screw make contact. Hence the gear ratio should be reworked. The Spring-fin (M2) model shows displacement in the spring facing downward, but no considerable deformation was observed in the top-facing spring/fin. These observations indicate that the bottom-facing spring was not fixed rigidly and hence requires correction. The stress beyond the benchmark was observed only in 4% of the total structure; hence it could be fixed.

The models M3 and M4 showed higher stability under all the applied loads, displaying a prospective result. Therefore, these implant designs could be taken for further biomechanical tests such as the effect on the implant, the spinal bones and the surrounding ligament muscles during specific motions like flexion, extension, etc. of the spine.

Funding: This research received no external funding
Acknowledgments: *Loyola-ICAM College of Engineering and Technology and *Sri Sivasubramaniya Nadar College of Engineering.
Conflicts of Interest: The authors declare no conflict of interest.

REFERENCES

1. Fatoye F, Gebrye T, Odeyemi, I. Real-world incidence and prevalence of low back pain using routinely collected data. Rheumatol Int. 2019; 39:619–26. doi.org/10.1007/s00296-019-04273-0
2. Rubin D I. Epidemiology and risk factors for spine pain. Neurol Clin. 2007; 25(2): 353-71. doi: 10.1016/j.ncl.2007.01.004.
3. Saleem S, Aslamm HM, Rehmani MA, Raees A, Alvi AA, Ashraf J. Lumbar disc degenerative disease: disc degeneration symptoms and magnetic resonance image findings. Asian Spine J. 2013; 7(4): 322-34. doi:10.4184/asj.2013.7.4.322
4. Medical Advisory Secretariat. Artificial discs for lumbar and cervical degenerative disc disease-update: An evidence-based analysis. Ont Health Technol Assess Ser. 2006; 6(10):1-98.
5. D'Souza M, Macdonald NA, Gendreau JL, Duddleston J, Feng AY, Ho AL. Graft Materials and Biologics for Spinal Interbody Fusion. Biomedicines. 2019; 7(4):75. doi:10.3390/biomedicines7040075
6. Calvo-Echenique A, Cegoñino J, Perez del PA. Is there any advantage of using stand-alone cages? A numerical approach. BioMed Eng. 2019; 18:63. https://doi.org/10.1186/s12938-019-0684-8
7. Mica MC, Voronov LI, Carandang G, Havey RM, Wojewnik B, Patwardhan AG. Biomechanics of an Expandable Lumbar Interbody Fusion Cage Deployed Through Transforaminal Approach. Int J Spine Surg. 2017;11:24. https://doi.org/10.14444/4024
8. Di Zhu, Duo Zhang, Baoge Liu, Chenxi Li, Jichao Zhu**,** Zhu D, et al. Can Self-Locking Cages Offer the Same Clinical Outcomes as Anterior Cage-with-Plate Fixation for 3-Level Anterior Cervical Discectomy and Fusion (ACDF) in Mid-Term Follow-Up? Med Sci Monit. 2019; 25: 547-557 DOI: 10.12659/MSM. 911234
9. Zhou SH, McCarthy ID, McGregor AH, Coombs RH, Hughes SPF. Geometrical dimensions of the lower lumbar vertebrae – analysis of data from digitized CT images. Eur Spine J. 2000; 9: 242–8.

10. Warburton A, Girdler SJ, Mikhail CM, Ahn A, Cho SK. Biomaterials in Spinal Implants: A Review. Neurospine. 2020;17:101–10. https://doi.org/10.14245/ns.1938296.148
11. Bowles RD, Setton L.A. Biomaterials for intervertebral disc regeneration and repair. Biomaterials. 2017; 129:54-67. doi: 10.1016/j.biomaterials.2017.03.013
12. Verma R, Virk S, Qureshi S. Interbody Fusions in the Lumbar Spine: A Review. HSS J. 2020;16:162-7. doi: 10.1007/s11420-019-09737-4.
13. Rao PJ, Pelletier MH, Walsh WR, Mobbs RJ. Spine interbody implants: material selection and modification, functionalization and bioactivation of surfaces to improve osseointegration. Orthop Surg. 2014;6:81-9. doi: 10.1111/os.12098.
14. Adam C, Pearcy M, McCombe P. Stress analysis of interbody fusion--finite element modeling of intervertebral implant and vertebral body. Clin Biomech (Bristol, Avon). 2003;18:265-72. doi: 10.1016/s0268-0033(03)00022-6.
15. Baumann AP, Graf T, Peck JH, Dmitriev AE, Coughlan D, Lotz JC. Assessing the use of finite element analysis for mechanical performance evaluation of intervertebral body fusion devices. JOR Spine. 2021;13:e1137. doi: 10.1002/jsp2.1137.
16. Fantigrossi A, Galbusera F, Raimondi MT, Sassi M, Fornari M. Biomechanical analysis of cages for posterior lumbar interbody fusion. Med Eng Phys. 2007;29:101-109. doi:10.1016/j.medengphy.2006.02.007
17. Schleicher P, Gerlach R, Schär B, Cain CM, Achatz W, Pflugmacher R, et al. Biomechanical comparison of two different concepts for stand alone anterior lumbar interbody fusion. Eur Spine J. 2008;17:1757-65. doi: 10.1007/s00586-008-0797-4.
18. Serra T, Capelli C, Toumpaniari R, Orriss IR, Leong JJH, Dalgarno K, et al. Design and fabrication of 3D-printed anatomically shaped lumbar cage for intervertebral disc (IVD) degeneration treatment. Biofabrication. 2016;8:035001. doi:10.1088/1758-5090/8/3/035001
19. Liu JT, Chen WC, Wei HW. Biomechanical evaluation of a dynamic fusion cage design for cervical spine: A finite element study. Adv Mech Eng. 2017; 9: 1–7. doi:10.1177/1687814017698881
20. Kavitha A, Sudhir G, Ranjani TS, Sarah Rajitha TV, Vinutha S. Implant Analysis on the Lumbar-Sacrum Vertebrae Using Finite Element Method. In: Wimpenny D, Pandey P, Kumar L. (eds) Advances in 3D Printing & Additive Manufacturing Technologies. Springer, Singapore. 2017. https://doi.org/10.1007/978-981-10-0812-2_13
21. Kavitha A, Sudhir G. Deepak V. Pavithra M, Vallabhi V. Analysis of Adjacent Vertebrae Post Vertebroplasty. 2019. doi:10.1007/978-981-13-0305-0_20.